Carbon 201 (2023) 535–541

Contents lists available at ScienceDirect

Carbon

journal homepage: www.elsevier.com/locate/carbon

Direct conversion of methane to zeolite-templated carbons, light hydrocarbons, and hydrogen

Yujie Liu [a,1], Elisabet Huertas Osta [a,1], Artem S. Poryvaev [b], Matvey V. Fedin [b], Alessandro Longo [c], Alexei Nefedov [d], Nikolay Kosinov [a,*]

[a] Laboratory of Inorganic Materials & Catalysis, Department of Chemical Engineering and Chemistry, Eindhoven University of Technology, P.O. Box 513, 5600 MB Eindhoven, the Netherlands
[b] International Tomography Center SB RAS and Novosibirsk State University, 630090, Novosibirsk, Russia
[c] European Synchrotron Radiation Facility, 71 Avenue des Martyrs, 38000 Grenoble, France and Istituto per lo Studio dei Materiali Nanostrutturati (ISMN)-CNR UOS Palermo, Via Ugo La Malfa, 153, 90146, Palermo, Italy
[d] Karlsruher Institut für Technologie (KIT), Institut für Funktionelle Grenzflächen (IFG), Hermann-von-Helmholtz-Platz 1, 76344 Eggenstein-Leopoldshafen, Germany

ARTICLE INFO

Keywords:
Methane conversion
Zeolite-templated carbons
Light hydrocarbons
Mo/ZSM-5
Zeolite topology

ABSTRACT

Efficient direct valorization of methane to value-added chemicals and materials remains an unsolved challenge for modern chemistry and materials science. In this work, we explored direct non-oxidative conversion of methane to hydrogen, hydrocarbons, and valuable zeolite-templated carbon materials. First, using a set of spectroscopy and microscopy characterization tools, we investigated how the reaction conditions influence the process of carbon formation inside the typical zeolite-based catalyst Mo/ZSM-5. Then, we explored the effect of the zeolite topology on the growth of carbon materials from methane decomposition over Mo/MFI, Mo/MOR, Mo/BEA, and Mo/FAU templates. Finally, we applied the obtained insights to prepare high-quality zeolite-templated carbons directly from methane using Fe/BEA and Fe/FAU templates. Altogether, our results represent a carbon-economic method of methane conversion to CO_x-free hydrogen gas, a mixture of light aliphatic and aromatic hydrocarbons, and valuable carbon materials.

1. Introduction

Direct valorization of abundant methane to value-added chemicals and materials remains an important problem for modern chemistry [1,2]. Non-oxidative catalytic conversion to solid carbon and CO_x-free H_2 gas is one of the most promising reactions to upgrade methane [3]. In this process, production of clean fuel (H_2) can be coupled with the fabrication of carbon-based materials in a highly atom-economic way [4]. The existing approaches of methane decomposition, with several exceptions [5–7], result in unstructured carbon materials that possess limited applicability. The value of the obtained carbon product is one of the key factors for the future commercial application of the catalytic methane decomposition [8]. A general challenge, here, is to find ways to effectively activate stable methane molecules and convert them to valuable ordered nanocarbons, without forming low-value graphitic compounds. Recently we found that coke, formed during non-oxidative dehydroaromatization of methane (MDA) over Mo/ZSM-5 catalysts, shows similar properties to zeolite-templated carbons (ZTCs) [9]. These materials are ordered microporous frameworks, consisting of sp^2-hybridized carbon atoms assembled in curved single-layer graphene moieties. ZTCs display long-range order, high surface area, chemical tunability, high conductivity, and elasticity. Thus, ZTCs are promising for a wide range of large-scale applications: gas storage [10,11], adsorption [12], and separation [13], CO_2 capture [14], solar evaporation [15], fluorophores [16], electrochemical capacitors [17,18], batteries [19], fuel cells [20], and electro-, photo- and thermal catalysis [21–23]. Previous studies show that, ZTCs can be produced by pyrolytic carbonization of organic precursors (typically acetylene, ethylene or furfuryl alcohol) inside the pores of zeolite templates, followed by dissolution of the zeolite and liberation of the resulting carbon material [24]. According to Kyotani and Nishihara, ZTCs can be classified into three types with respect to their quality [25]. Type-I corresponds to ZTC materials, representing 3D-ordered inverted replica of the zeolite structure. ZTCs of Type-I are characterized by high surface area (>2100

* Corresponding author.
E-mail address: n.a.kosinov@tue.nl (N. Kosinov).
[1] These authors contributed equally.

https://doi.org/10.1016/j.carbon.2022.09.050
Received 30 June 2022; Received in revised form 4 September 2022; Accepted 15 September 2022
Available online 19 September 2022

m^2/g); presence of ordered structure, as indicated by X-ray diffraction (XRD) peaks corresponding to zeolite d-spacing; and absence of graphene stacking, as indicated by XRD peaks of graphite. ZTCs of Type II are characterized by some degree of ordering, but either contain graphene stacking defects or possess surface area lower than 2100 m^2/g. Finally, ZTCs of Type-III are microporous carbons that do not possess obvious ordered structure. In this work, aiming to bring value to the material side of methane conversion, we explore the synthesis of high-quality ZTCs directly from methane. In order to realize this carbon-economic process, we focused on the effects of reaction conditions, zeolite topology, and transition-metal catalytic function required for methane activation.

2. Experimental methods

2.1. Preparation of zeolite templates

Commercial zeolites NH_4ZSM-5 (Alfa Aesar, Si/Al = 25), HY (FAU, Alfa Aesar, Si/Al = 2.6), HBEA (BEA, Zeolyst, Si/Al = 12) and NH_4MOR (MOR, Zeolyst, Si/Al = 15) were used in this work. NH_4ZSM-5 and NH_4MOR were converted to proton form by calcination at 550 °C for 4 h. The zeolite powders were loaded with 1 wt% Mo by incipient wetness impregnation with aqueous solution of ammonium heptamolybdate tetrahydrate (Sigma Aldrich, $(NH_4)_6Mo_7O_{24}{\cdot}4H_2O$) at room temperature. Additionally, Fe/BEA and Fe/FAU were prepared with 1 wt% loading of Fe by incipient wetness impregnation with aqueous solution of ferric nitrate nonahydrate (Sigma Aldrich, $Fe(NO_3)_3{\cdot}9H_2O$) at room temperature. After impregnation, Mo/zeolite and Fe/zeolite catalysts were dried overnight at 110 °C and calcined at 550 °C for 8 h at a ramp rate of 2 °C/min. The samples were pelletized, crushed with a mortar and a pestle, and finally sieved to achieve a pellet fraction of 250–500 μm.

2.2. Carbonization of zeolite templates and liberation of carbon materials

Carbonization of metal-modified zeolite templates by methane was performed in a flow setup. For each experiment, 0.5 g of the catalyst sample was loaded in a fixed-bed quartz reactor (i.d. 4.0 mm, o.d. 8 mm, length 450 mm). The reactions were performed in a continuous flow of 50 mL/min of CH_4:N_2 (95:5) mixture. The product composition was analyzed by a gas chromatograph (Compact GC, Interscience). In the experiments, the reactor was heated up to 450 °C at a ramp rate of 10 °C/min, followed by an isothermal step for 45 min to remove physisorbed compounds from the zeolite pores. Afterwards, the reactor was heated to the specified reaction temperature (625–750 °C) at a ramp rate of 15 °C/min and held for 960 min (unless stated otherwise) at this temperature. Once the reaction was finished, the reactor was cooled down to room temperature and the carbonized zeolite sample was recovered.

In order to liberate the carbon material from the pores, the carbonized zeolites were treated by hydrofluoric acid (HF). HF is a highly toxic compound, so these experiments need to be performed with caution and suitable personal protection equipment should be used. For experiments, aqueous solution of HF (40 wt%) was added to the carbonized samples (5 $g_{solution}$/1 g_{sample}). After stirring the obtained mixture for 2 h at room temperature, it was filtered on a paper filter and the solid residue was then washed thoroughly with deionized water. The obtained carbon samples were dried overnight at 110 °C.

2.3. Characterization of materials

Carbonized zeolite templates and liberated carbon materials were characterized by a range of physical-chemical techniques listed below.

X-ray diffraction (XRD). XRD patterns were recorded with a Bruker D2 Phaser powder diffractometer equipped with a Cu Kα x-ray source (scan speed 0.01°/s, 2θ range 5–50°).

Near edge X-ray absorption fine structure (NEXAFS). NEXAFS spectra of synthesized carbon materials were recorded at HE-SGM beamline of BESSY II synchrotron (Berlin, Germany) [26]. NEXAFS spectra were recorded at the carbon K-edge in a partial electron yield mode with retarding voltage of −150 V. As the primary X-ray source, linearly polarized synchrotron light with a polarization factor of ~91% was used. The incidence angle of the X-rays was kept at 55° ("magic angle"). The photon energy (PE) scale at the C K-edge was referenced to the pronounced π* resonance of highly oriented pyrolytic graphite at 285.38 eV. The spectra were corrected for the PE dependence of the incident photon flux by division through the spectrum of clean gold and reduced to the standard form (zero intensity in the pre-edge region and the unity jump in the far post-edge region).

X-ray Raman scattering (XRS). XRS spectrum of carbonized Mo/ZSM-5 template was recorded at ID20 beamline of ESRF synchrotron (Grenoble, France). The pink beam from four U26 undulators was monochromatized, by a cryogenically cooled Si (111) monochromator and focused to a spot size of approximately 50 μm × 50 μm (V × H) at the sample position with a mirror system in Kirkpatrick-Baez geometry. The large solid angle spectrometer at ID20 was used to collect XRS data with 36 spherically bent Si (660) analyzer crystals [27]. The data were treated with the XRS program package as described elsewhere [28]. The powder samples were put in a capillary, and then measured in transmission geometry. Measurements were performed at room temperature. All scans were checked for the radiation damage by changing the sample position during the measurement.

Raman spectroscopy. Raman spectra were recorded with a Witec Alpha 300 confocal Raman microscope equipped with a 532 nm laser.

Ar adsorption. Textural properties of materials were analyzed by Ar physisorption carried out at −186 °C with a Micromeritics ASAP-2020 apparatus. Surface area was estimated by the BET model and microporous volume was estimated by the *t*-plot model. Prior to the measurements the samples were pretreated at 300 °C in vacuum.

Electron microscopy. The morphology of the zeolite and carbon particles was analyzed by scanning electron microscopy (SEM) with a Phenom World Pro Desktop scanning electron microscope at an accelerating voltage of 3–5 kV. Transmission electron microscopy (TEM) micrographs were obtained with a FEI Tecnai 20 instrument at an electron acceleration voltage of 200 kV. The samples for TEM were prepared by suspending carbon materials in ethanol and placing a drop of the suspension onto holey copper grid covered with carbon film.

Thermogravimetric analysis (TGA). Thermogravimetric analysis (TGA) of prepared materials was performed with a Mettler Toledo TGA/DSC 1 instrument. About 20 mg of carbonized zeolite templates and about 2 mg of carbon materials was placed in uncovered alumina crucible, which was heated to 800 °C at a rate of 5 °C/min in a 40 mL/min He + 20 mL/min O_2 flow.

Electron paramagnetic resonance (EPR) spectroscopy. EPR spectra of carbon materials were recorded with a Bruker Elexsys E580 X/Q-band EPR spectrometer equipped with a temperature control system (Oxford Instruments, T = 4–300 K). Powdered samples were placed into quartz sample tubes (OD = 3.8 mm). Dielectric X-band resonator ER 4118 X-MD5 has inherent Mo (III) impurities in the sapphire ring, giving signal outside the spectral region of interest and, therefore, convenient as a reference. The number of spins in this reference signal was determined by measuring a model solution of stable TEMPO radical. X-band CW EPR measurements with this inherent reference allowed us to estimate the number of radicals in each sample. To assess possible influence of exchange couplings on the apparent spin concentration of radicals, the X0-band continuous wave (CW) EPR spectra for all samples were obtained at temperatures between 80 and 200 K. The apparent radical concentration was found similar in this temperature range for each sample.

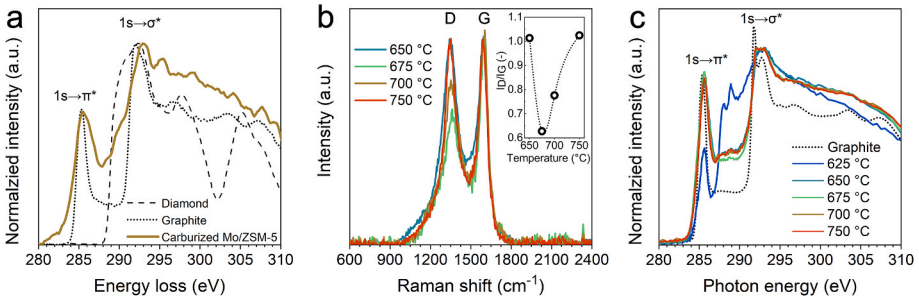

Fig. 1. Effect of reaction temperature on the properties of carbon formed in Mo/ZSM-5 during non-oxidative conversion of methane. **a)** X-ray Raman spectrum (excitation energy 10 keV) of carbonized Mo/ZSM-5 sample treated in methane flow at 700 °C for 16 h together with diamond and graphite reference spectra. **b)** Raman spectra (λ = 532 nm) of carbonized Mo/ZSM-5 samples treated in methane flow at different temperatures for 16 h, inset shows the intensity ratio between D- and G-bands. **c)** NEXAFS spectra of carbon materials liberated from carbonized Mo/ZSM-5 samples together with graphite reference spectrum. (A colour version of this figure can be viewed online.)

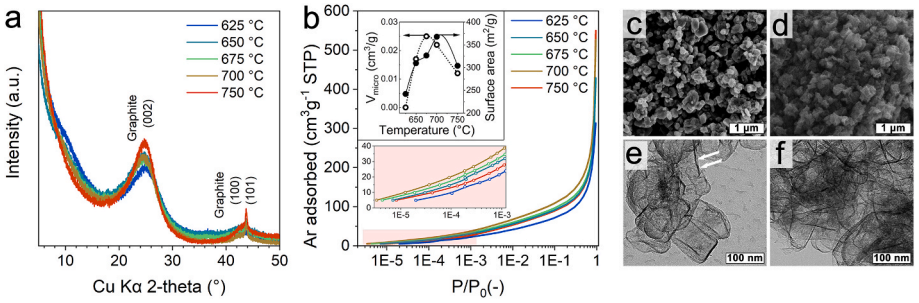

Fig. 2. a) XRD patterns of liberated carbon materials obtained at different temperature. **b)** Ar adsorption isotherms and textural properties of liberated carbon materials. **c)** SEM image of Mo/ZSM-5 sample after methane treatment at 700 °C. **d)** SEM image of carbon material liberated from Mo/ZSM-5 after methane treatment at 700 °C. TEM images of carbon material liberated from Mo/ZSM-5 after methane treatment at **e)** 700 °C and **f)** 750 °C. (A colour version of this figure can be viewed online.)

3. Results and discussion

3.1. Conversion of methane over Mo/ZSM-5 templates

First, we studied a conventional MDA catalyst Mo/ZSM-5 and assessed the potential temperature window for the direct methane-to-ZTCs reaction. For this purpose, we carbonized 1%Mo/ZSM-5 template in a flow of methane (50 mL/min) for 16 h at varying temperature (625–750 °C). The results show that the amount of formed carbon increases with increasing the reaction temperature (Fig. S1). To probe the structure of deposited carbon inside the zeolite pores, X-ray Raman scattering (XRS) was employed. XRS has recently attracted widespread attention in materials science due to its unique capabilities: it allows analyzing low-energy X-ray absorption edges, such as carbon K-edge (≈280 eV), using hard X-rays for both excitation and signal collection [28]. The use of XRS solves common problems associated with soft X-ray techniques, such as X-ray absorption fine structure (NEXAFS) spectroscopy and X-ray photoelectron spectroscopy (XPS), namely the low bulk sensitivity and the need to use vacuum. Fig. 1a shows an XRS spectrum of carbon, formed inside the pores of Mo/ZSM-5, after carbonization at 700 °C for 16 h. The peak at 285.5 eV corresponds to transition of 1s electron to empty π* states, and peaks above 290 eV correspond to 1s→σ* transitions [29]. The spectrum of carbonized Mo/ZSM-5 shows that, in line with the structure of ZTC, the carbon material formed inside the zeolite pores is mainly sp^2 hybridized [30,31]. Vibrational Raman spectra of carbonized Mo/ZSM-5 samples (Fig. 1b) display typical for ZTC materials features: G band at around 1598 cm^{-1} and D band at around 1345 cm^{-1} [32]. The G band is related to the graphitic/graphene lattice vibration mode with E_{2g} symmetry and the D band is related to the presence of defects or disorder in graphitic and graphene materials [33]. The D/G ratios (Fig. 1b inset) of carbonized Mo/ZSM-5 samples have a minimum at 675 °C, likely indicating that the least defective ZTC structure was obtained at this carbonization temperature. Next, we dissolved the carbonized Mo/ZSM-5 samples in HF (the efficiency of the dissolution procedure is confirmed by TG analysis on Fig. S1), collected the obtained carbon materials, and analyzed them by NEXAFS (Fig. 1c). The results demonstrate that formed ZTC materials, except for the sample obtained at 625 °C, mainly consist of sp^2-hybridized carbon atoms with a certain fraction of C–H and/or C–O bonds as manifested by peaks between 287 and 291 eV. These peaks correspond to extended Rydberg-type final states [34]. The NEXAFS spectrum of liberated ZTC obtained at 700 °C is similar to the XRS spectrum of the corresponding carbonized Mo/ZSM-5 sample. This finding confirms that the structure of the material is preserved during the dissolution of the zeolite matrix.

XRD patterns of MFI-ZTC materials (Fig. 2a) display no obvious ordering and only peaks related to graphene stacking are observed. With increasing carbonization temperature, the degree of graphitization increases. These findings are in line with the EPR spectroscopy data, showing that the concentration of radicals (unpaired electron spins) in MFI-ZTC materials decreases with increasing carbonization temperature (Fig. S2). Indeed, ordered ZTC materials are known to contain radicals in their structure (dangling bonds, unsaturated edges, radical spins localized on negatively curved graphene fragments) [31,35,36]. The higher extent of graphitization on the external surface of zeolite crystals leads to a lower overall number of ZTC-related radical spins. As shown by Fig. 2b, the liberated ZTC materials are microporous carbons with an optimum in BET surface area (370 m^2/g) when prepared at 700 °C, and the optimum in microporous volume (0.03 cm^3/g) was observed for the one synthesized at 675 °C. SEM analysis (Fig. 2c and d) confirms the particulate nature of the prepared ZTC materials, and TEM analysis (Fig. 2e and f) demonstrates presence of graphene stacking on the external surface of the particulates. We notice that TEM results correlate well with XRD and EPR analysis, as the highest amount of graphene stacking/graphitization of ZTC material was observed when increasing the temperature to 750 °C. To investigate the influence of Mo loading on the formation of ZTC materials, we prepared 2% Mo/ZSM-5 template and treated it in methane flow at 675–700 °C. We show that, for 1% Mo/ZSM-5 and 2% Mo/ZSM-5 templates, the amount of formed carbon does not significantly depend on Mo loading (Fig. S3). We also obtained comparable Type-III ZTC materials (presence of graphene stacking, low degree of ordering) with both templates (Fig. S4). We conclude that the influence of the Mo loading on methane-to-ZTC reaction is minor. To summarize, we were able to obtain Type-III ZTC materials from methane using conventional MDA catalyst – Mo/ZSM-5. We also identified the suitable temperature window for the methane-to-ZTC reaction (675–700 °C) (see Fig. 2).

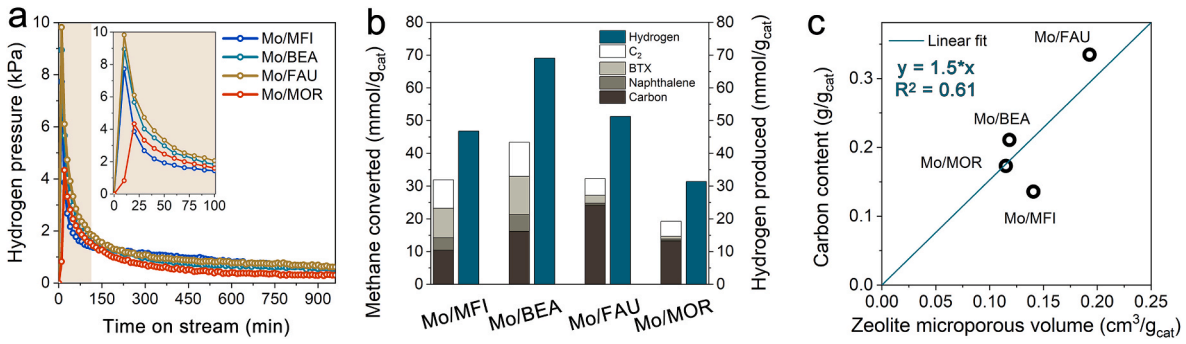

Fig. 3. Effect of zeolite topology on the performance of respective Mo/zeolite catalysts in non-oxidative conversion. **a)** Evolution of hydrogen pressure with time-on-stream in methane flow (50 mL/min) at 700 °C. **b)** Total distribution of hydrocarbon products and hydrogen formed during methane conversion experiments. **c)** Microporous volume of Mo/zeolite catalysts and the amount of carbon formed over these catalysts after treatment in methane at 700 °C. (A colour version of this figure can be viewed online.)

3.2. Effect of zeolite topology

Zeolite topology plays a key role in the formation of zeolite-templated carbons [37]. In line with previous reports, we could only obtain ZTC materials of Type-III using MFI templates with medium-sized 10MR pores [38]. Next, we decided to investigate three other topologies with larger 12MR pores: BEA, FAU and MOR. These commercialized zeolites have been previously used for the synthesis of ZTC materials from olefin or furfuryl alcohol precursors [39]. We prepared the corresponding Mo-modified templates and compared their performance in non-oxidative methane conversion at 700 °C. The catalytic results onFig. 3a,b and S5 demonstrate that conversion of methane over these materials strongly depends on the zeolite topology. While Mo/MFI and Mo/BEA templates display high carbon selectivity towards aromatic and aliphatic hydrocarbons (~60%), solid carbon is the main product formed over Mo/FAU and Mo/MOR with the selectivity to carbon of ~70% (Fig. S5b). The total amount of formed carbon correlates with the microporous volume of the zeolite templates, particularly 12MR ones, indicating the preferential growth of carbon inside the pores (Fig. 3c). A lower amount of carbon formed in the Mo/MFI template can be explained by the incomplete filling of smaller 10MR pores. The XRD patterns of the carbonized templates display distinct differences as compared to the XRD patterns of as-prepared templates (Fig. S6). This finding further confirms the deposition of carbonaceous molecules inside the zeolite pores, which leads to changes in XRD patterns [40]. The highest carbon loading (~0.35$g_{carbon}/g_{catalyst}$) was observed for the Mo/FAU template (Fig. 3c and S7). We then dissolved the carbonized Mo/FAU template in HF and characterized the obtained FAU-ZTC material by NEXAFS, XRD, Ar adsoption and electron microscopy (Fig. S8). The results demonstrate that carbon material, obtained from decomposition of methane over Mo/FAU, is a Type-II ZTC. This material mainly consists of sp^2-hybridized carbon atoms and displays a characteristic XRD peak at 6.3° and surface area of 1360 m^2/g (Figs. S8a-c). A significant fraction of graphene stacking on the external surface was also observed (Fig. S8f).

3.3. High-quality ZTC materials from Fe/BEA and Fe/FAU templates

In order to further improve the quality of methane-derived ZTC materials, we have prepared Fe-modified Fe/BEA and Fe/FAU zeolite templates. We hypothesized that, since Fe is less active for methane activation than Mo [41], it will lead to a slower growth of carbon inside the zeolite pores and may accordingly result in a better quality of ZTCs. The Fe/BEA and Fe/FAU templates were prepared by incipient wetness impregnation of commercial BEA (Si/Al = 12) and FAU (Si/Al = 2.6) materials with 1 wt% Fe.

To optimize the carbonization time for these Fe/zeolite templates, we first tested Fe/FAU template in methane flow of 50 mL/min and at 675 °C for 16 h, 2 days and 4 days, respectively (Figs. S9, S10 and discussion therein). The results show that ZTC materials can be obtained with Fe/FAU zeolite templates and that 2–3 days for carbonization is optimal. Thus, the prepared Fe/BEA and Fe/FAU templates were slowly carbonized in methane flow at 675 °C for 3 days. Solid carbon and hydrogen were the main reaction products (Fig. S11). We should note that, in contrast to Fe/FAU with 95% selectivity to solid carbon, Fe/BEA also demonstrated significant C_2 (23.2%) and aromatic (12.3%) selectivity (Fig. S11c).

After carbonization, the zeolite templates were dissolved by HF and

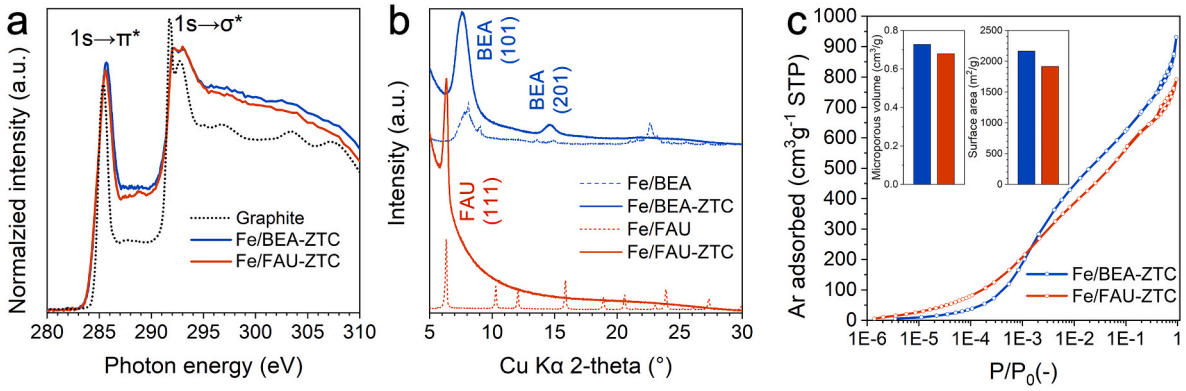

Fig. 4. Synthesis of high-quality ZTC materials from methane with Fe/BEA and Fe/FAU templates. **a)** NEXAFS spectra of ZTC materials liberated from carbonized Fe/FAU and Fe/BEA together with graphite reference spectrum. **b)** XRD patterns of ZTC materials, dashed patterns correspond to the fresh Fe/BEA and Fe/FAU templates. **c)** Ar adsorption isotherms and textural properties of ZTC materials. (A colour version of this figure can be viewed online.)

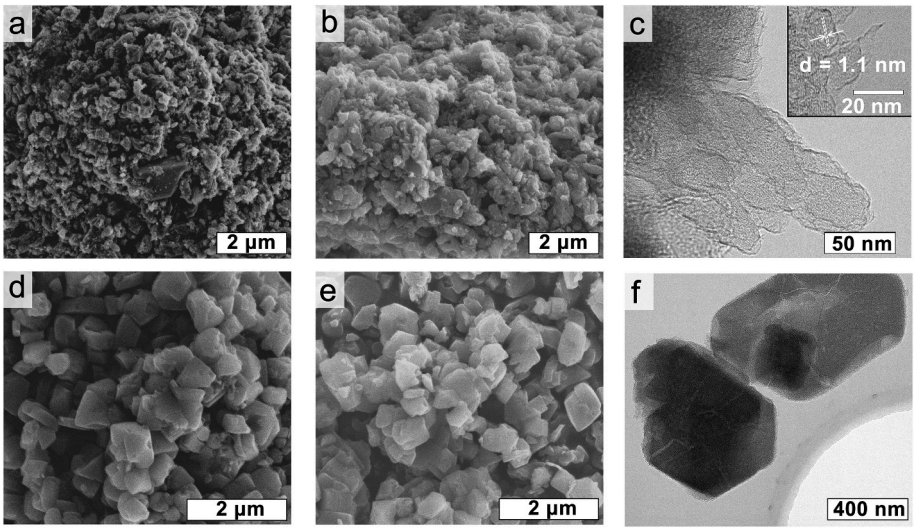

Fig. 5. SEM images of **a)** carbonized Fe/BEA and **d)** carbonized Fe/FAU. SEM images of **b)** Fe/BEA-ZTC and **e)** Fe/FAU-ZTC. TEM images of **c)** Fe/BEA-ZTC and **f)** Fe/FAU-ZTC. (A colour version of this figure can be viewed online.)

the obtained ZTCs were characterized. Carbon K-edge NEXAFS spectra of BEA-ZTC and FAU-ZTC are characterized by a sharp 1s→π* transition at 285.6 eV, several 1s→σ* transitions at 292–295 eV (Fig. 4a). The spectra confirm that the majority of carbon atoms in BEA-ZTC and FAU-ZTC are of sp^2 nature, and that the number of C–H and C–O bonds in the obtained materials (Rydberg-type orbitals between 287 and 291 eV) is low. XRD patterns of Fe/FAU-ZTC display a sharp reflection at $2\theta = 6.3^\circ$ (d spacing = 1.4 nm). XRD pattern of Fe/BEA-ZTC demonstrates two reflections at 7.6° (d spacing = 1.1 nm) and 14.6° (Fig. 4b). These reflections correspond to the FAU (111) and BEA (101) and (201) planes of the initial zeolite templates, respectively, and indicate the presence of ordered carbon structure [42]. No significant graphene stacking was observed in XRD patterns of Fe/BEA-ZTC and Fe/FAU-ZTC (Fig. 4b). Ar adsorption isotherms demonstrate the microporous nature of the obtained ZTC materials with high microporous volume (0.68–0.73 cm^3/g) and surface area (1900–2200 m^2/g) values (Fig. 4c).

Similar morphology of the carbonized zeolite templates and liberated ZTC materials was observed by SEM (Fig. 5a,b,d,e). Finally, TEM images show that the formed ZTCs are composed of uniform carbon particles without significant graphene stacking on the external surface (Fig. 5c,f). The observed interatomic distance for BEA-ZTC (1.1 nm) corresponds well to the XRD peak observed at $2\theta = 7.6^\circ$. Obtained results confirm the high quality of the ZTC materials, belonging to ZTC type-I in classification of Nishihara and Kyotani.

To summarize, we identified a suitable combination of reaction conditions and metal-modified zeolite templates that allowed us to prepare high-quality ZTC materials directly from methane. The transition metal catalyst function, zeolite topology and reaction temperature are the key parameters influencing the conversion of methane into ZTCs. Here, we should note, that the loss of the zeolite templates is the fundamental disadvantage of the proposed process. There are several potential solutions to this problem, including, using cheaper templates [43], waste zeolite materials (i.e. spent FCC catalysts [44] or zeolite materials produced from industrial waste [45]), and even recycling of the zeolite template. Indeed, the products of aluminosilicate dissolution in HF or NaOH [46] are a mixture of sodium silicate/sodium aluminate or fluorosilicate/fluoroaluminate compounds. Such mixtures are either directly suitable for the hydrothermal synthesis of zeolites or can be made suitable just by adding an organic structure-directing agent (e.g., tetrapropylammonium hydroxide for the synthesis of MFI zeolite) [47]. The successful recycling of the zeolite template will lead to the reduction of the waste and enhancement of the overall atom efficiency of the process. This can potentially promote the fabrication of methane-derived ZTCs from an academic novelty to a commercially relevant process.

4. Conclusions

In this work we showed that coke forming over metal-modified zeolite catalysts during conversion of methane is not necessarily a waste. The growth of carbon from methane inside the zeolite pores can be directed to obtain high-quality zeolite-templated carbons. In addition to the value-added carbon materials, CO_x-free hydrogen, light olefins and aromatics are also produced, resulting in a high overall atom-efficiency of the process. Zeolite templates based on BEA zeolite are particularly promising for the simultaneous production of high-quality ZTCs and hydrocarbons. Since existing indirect methane conversion routes suffer from high capital costs, the atom-economic direct conversion of methane to valuable carbon materials, hydrocarbons, and hydrogen might be a promising solution for the widespread remote and small methane sources.

CRediT authorship contribution statement

Yujie Liu: Investigation, Writing – review & editing. **Elisabet Huertas Osta:** Investigation, Writing – original draft. **Artem S. Poryvaev:** Investigation. **Matvey V. Fedin:** Investigation. **Alessandro Longo:** Investigation. **Alexei Nefedov:** Investigation. **Nikolay Kosinov:** Conceptualization, Supervision, Investigation, Writing - review & editing.

Declaration of competing interest

The authors declare that they have no known competing financial interests or personal relationships that could have appeared to influence the work reported in this paper.

Acknowledgements

Financial support from China Scholarship Council (201806930028) is gratefully acknowledged. This publication is part of the project OCENW.XS21.3.019 which is financed by the Dutch Research Council (NWO). We acknowledge the European Synchrotron Radiation Facility for provision of synchrotron radiation facilities. The Helmholtz Zentrum Berlin is gratefully acknowledged for beamtime allocation.

Appendix A. Supplementary data

Supplementary data related to this article can be found at https://doi.org/10.1016/j.carbon.2022.09.050.

References

[1] A.I. Olivos-Suarez, À. Szécsényi, E.J.M. Hensen, J. Ruiz-Martinez, E.A. Pidko, J. Gascon, Strategies for the direct catalytic valorization of methane using heterogeneous catalysis: challenges and opportunities, ACS Catal. 6 (2016) 2965–2981, https://doi.org/10.1021/acscatal.6b00428.

[2] P. Schwach, X. Pan, X. Bao, Direct conversion of methane to value-added chemicals over heterogeneous catalysts: challenges and prospects, Chem. Rev. 117 (2017) 8497–8520, https://doi.org/10.1021/acs.chemrev.6b00715.

[3] H.F. Abbas, W.M.A. Wan Daud, Hydrogen production by methane decomposition: a review, Int. J. Hydrogen Energy 35 (2010) 1160–1190, https://doi.org/10.1016/j.ijhydene.2009.11.036.

[4] D.C. Upham, V. Agarwal, A. Khechfe, Z.R. Snodgrass, M.J. Gordon, H. Metiu, E. W. McFarland, Catalytic molten metals for the direct conversion of methane to hydrogen and separable carbon, Science 358 (2017) 917–921, https://doi.org/10.1126/science.aao5023.

[5] Y. Lv, Z. Wu, Y. Fang, X. Qian, A.M. Asiri, B. Tu, D. Zhao, Hierarchical mesoporous/microporous carbon with graphitized frameworks for high-performance lithium-ion batteries, APL Mater. 2 (2014) 113302-1–113302-7, https://doi.org/10.1063/1.4897201.

[6] Z. Wu, Y. Yang, D. Gu, Y. Zhai, D. Feng, Q. Li, B. Tu, P.A. Webley, D.Y. Zhao, Synthesis of ordered mesoporous carbon materials with semi-graphitized walls via direct in-situ silica-confined thermal decomposition of CH4 and their hydrogen storage properties, Top. Catal. 52 (2009) 12–26, https://doi.org/10.1007/s11244-008-9134-8.

[7] H. Nishihara, T. Simura, S. Kobayashi, K. Nomura, R. Berenguer, M. Ito, M. Uchimura, H. Iden, K. Arihara, A. Ohma, Y. Hayasaka, T. Kyotani, Oxidation-resistant and elastic mesoporous carbon with single-layer graphene walls, Adv. Funct. Mater. (2016) 6418–6427, https://doi.org/10.1002/adfm.201602459.

[8] T. Marquardt, A. Bode, S. Kabelac, Hydrogen production by methane decomposition: analysis of thermodynamic carbon properties and process evaluation, Energy Convers. Manag. 221 (2020), 113125, https://doi.org/10.1016/j.enconman.2020.113125.

[9] N. Kosinov, E.A. Uslamin, F.J.A.G. Coumans, A.S.G. Wijpkema, R.Y. Rohling, E.J. M. Hensen, Structure and evolution of confined carbon species during methane dehydroaromatization over Mo/ZSM-5, ACS Catal. 8 (2018) 8459–8467, https://doi.org/10.1021/acscatal.8b02491.

[10] N.P. Stadie, J.J. Vajo, R.W. Cumberland, A.A. Wilson, C.C. Ahn, B. Fultz, Zeolite-templated carbon materials for high-pressure hydrogen storage, Langmuir 28 (2012) 10057–10063, https://doi.org/10.1021/la302050m.

[11] E. Masika, R. Mokaya, Exceptional gravimetric and volumetric hydrogen storage for densified zeolite templated carbons with high mechanical stability, Energy Environ. Sci. 7 (2014) 427–434, https://doi.org/10.1039/c3ee42239a.

[12] S.K. Lee, H. Park, J.W. Yoon, K. Kim, S.J. Cho, G. Maurin, R. Ryoo, J.S. Chang, Microporous 3D graphene-like zeolite-templated carbons for preferential adsorption of ethane, ACS Appl. Mater. Interfaces 12 (2020) 28484–28495, https://doi.org/10.1021/acsami.0c04228.

[13] S.K. Lee, H. Park, K. Cho, J.M. Park, R. Ryoo, U.H. Lee, J.S. Chang, Nanoporous 3D graphene-like zeolite-templated carbon for high-affinity separation of xenon from krypton, ACS Appl. Nano Mater. (2022), https://doi.org/10.1021/acsanm.2c00860.

[14] S. Builes, T. Roussel, C.M. Ghimbeu, J. Parmentier, R. Gadiou, C. Vix-Guterl, L. F. Vega, Microporous carbon adsorbents with high CO_2 capacities for industrial applications, Phys. Chem. Chem. Phys. 13 (2011) 16063–16070, https://doi.org/10.1039/c1cp21673b.

[15] J. Wang, Z. Liu, X. Dong, C.E. Hsiung, Y. Zhu, L. Liu, Y. Han, Microporous cokes formed in zeolite catalysts enable efficient solar evaporation, J. Mater. Chem. A. 5 (2017) 6860–6865, https://doi.org/10.1039/C7TA00882A.

[16] S.H. Ko, T. Lee, H. Park, D.S. Ahn, K. Kim, Y. Kwon, S.J. Cho, R. Ryoo, Nanocage-Confined synthesis of fluorescent polycyclic aromatic hydrocarbons in zeolite, J. Am. Chem. Soc. 140 (2018) 7101–7107, https://doi.org/10.1021/jacs.8b00900.

[17] C. Portet, Z. Yang, Y. Korenblit, Y. Gogotsi, R. Mokaya, G. Yushin, Electrical double-layer capacitance of zeolite-templated carbon in organic electrolyte, J. Electrochem. Soc. 156 (2009) A1, https://doi.org/10.1149/1.3002375.

[18] H. Itoi, H. Nishihara, T. Kogure, T. Kyotani, Three-dimensionally arrayed and mutually connected 1.2-nm nanopores for high-performance electric double layer capacitor, J. Am. Chem. Soc. 133 (2011) 1165–1167, https://doi.org/10.1021/ja108315p.

[19] N.P. Stadie, S. Wang, K.V. Kravchyk, M.V. Kovalenko, Zeolite-templated carbon as an ordered microporous electrode for aluminum batteries, ACS Nano 11 (2017) 1911–1919, https://doi.org/10.1021/acsnano.6b07995.

[20] F. Su, J. Zeng, Y. Yu, L. Lv, J.Y. Lee, X.S. Zhao, Template synthesis of microporous carbon for direct methanol fuel cell application, Carbon 43 (2005) 2366–2373, https://doi.org/10.1016/j.carbon.2005.04.018.

[21] C.H. Choi, M. Kim, H.C. Kwon, S.J. Cho, S. Yun, H.T. Kim, K.J.J. Mayrhofer, H. Kim, M. Choi, Tuning selectivity of electrochemical reactions by atomically dispersed platinum catalyst, Nat. Commun. 7 (2016) 1–9, https://doi.org/10.1038/ncomms10922.

[22] W. Donphai, T. Kamegawa, M. Chareonpanich, K. Nueangnoraj, H. Nishihara, T. Kyotani, H. Yamashita, Photocatalytic performance of TiO_2-zeolite templated carbon composites in organic contaminant degradation, Phys. Chem. Chem. Phys. 16 (2014) 25004–25007, https://doi.org/10.1039/c4cp03897e.

[23] P.W. Chung, M. Yabushita, A.T. To, Y. Bae, J. Jankolovits, H. Kobayashi, A. Fukuoka, A. Katz, Long-chain glucan adsorption and depolymerization in zeolite-templated carbon catalysts, ACS Catal. 5 (2015) 6422–6425, https://doi.org/10.1021/acscatal.5b01172.

[24] K. Kim, T. Lee, Y. Kwon, Y. Seo, J. Song, J.K. Park, H. Lee, J.Y. Park, H. Ihee, S. J. Cho, R. Ryoo, Lanthanum-catalysed synthesis of microporous 3D graphene-like carbons in a zeolite template, Nature 535 (2016) 131–135, https://doi.org/10.1038/nature18284.

[25] H. Nishihara, T. Kyotani, Zeolite-templated carbons-three-dimensional microporous graphene frameworks, Chem. Commun. 54 (2018) 5648–5673, https://doi.org/10.1039/c8cc01932k.

[26] A. Nefedov, C. Wöll, Advanced applications of NEXAFS spectroscopy for functionalized surfaces, Springer Ser. Surf. Sci. 51 (2013) 277–303, https://doi.org/10.1007/978-3-642-34243-1_11.

[27] M.M. Sala, K. Martel, C. Henriquet, A. Al Zein, L. Simonelli, C.J. Sahle, H. Gonzalez, M.C. Lagier, C. Ponchut, S. Huotari, R. Verbeni, M. Krisch, G. Monaco, A high-energy-resolution resonant inelastic X-ray scattering spectrometer at ID20 of the European Synchrotron Radiation Facility, J. Synchrotron Radiat. 25 (2018) 580–591, https://doi.org/10.1107/S1600577518001200.

[28] C.J. Sahle, A. Mirone, J. Niskanen, J. Inkinen, M. Krisch, S. Huotari, Planning, performing and analyzing X-ray Raman scattering experiments, J. Synchrotron Radiat. 22 (2015) 400–409, https://doi.org/10.1107/S1600577514027581.

[29] C. Cavallari, M. Brunelli, S. Radescu, M. Dubois, N. Batisse, G.B.M. Vaughan, H. E. Fischer, V. Pischedda, Structural and electronic changes in graphite fluorides as a function of fluorination rate: an XRS, PDF and DFT study, Carbon 147 (2019) 1–8, https://doi.org/10.1016/j.carbon.2019.02.053.

[30] R. Georgiou, P. Gueriau, C.J. Sahle, S. Bernard, A. Mirone, R. Garrouste, U. Bergmann, J.P. Rueff, L. Bertrand, Carbon speciation in organic fossils using 2D to 3D x-ray Raman multispectral imaging, Sci. Adv. 5 (2019) 1–10, https://doi.org/10.1126/sciadv.aaw5019.

[31] K. Takai, T. Suzuki, T. Enoki, H. Nishihara, T. Kyotani, Fabrication and characterization of magnetic nanoporous zeolite templated carbon, J. Phys. Chem. Solid. 71 (2010) 565–568, https://doi.org/10.1016/j.jpcs.2009.12.037.

[32] H. Nishihara, Q.H. Yang, P.X. Hou, M. Unno, S. Yamauchi, R. Saito, J.I. Paredes, A. Martínez-Alonso, J.M.D. Tascón, Y. Sato, M. Terauchi, T. Kyotani, A possible buckybowl-like structure of zeolite templated carbon, Carbon 47 (2009) 1220–1230, https://doi.org/10.1016/j.carbon.2008.12.040.

[33] A. Sadezky, H. Muckenhuber, H. Grothe, R. Niessner, U. Pöschl, Raman microspectroscopy of soot and related carbonaceous materials: spectral analysis and structural information, Carbon 43 (2005) 1731–1742, https://doi.org/10.1016/j.carbon.2005.02.018.

[34] M. Klues, K. Hermann, G. Witte, Analysis of the near-edge X-ray-absorption fine-structure of anthracene: a combined theoretical and experimental study, J. Chem. Phys. 140 (2014), https://doi.org/10.1063/1.4855215.

[35] K. Takai, T. Suzuki, H. Nishihara, T. Kyotani, T. Enoki, Magnetic properties of host-guest material using network of curved nanocarbon sheet, J. Phys. Chem. Solid. 73 (2012) 1436–1439, https://doi.org/10.1016/j.jpcs.2012.02.032.

[36] A. Gabe, M. Ouzzine, E.E. Taylor, N.P. Stadie, N. Uchiyama, T. Kanai, Y. Nishina, H. Tanaka, Z.Z. Pan, T. Kyotani, H. Nishihara, High-density monolithic pellets of double-sided graphene fragments based on zeolite-templated carbon, J. Mater. Chem. A. 9 (2021) 7503–7507, https://doi.org/10.1039/d0ta11625d.

[37] E. Braun, Y. Lee, S.M. Moosavi, S. Barthel, R. Mercado, I.A. Baburin, D. M. Proserpio, B. Smit, Generating carbon schwarzites via zeolite-templating, Proc. Natl. Acad. Sci. U.S.A. 115 (2018) E8116, https://doi.org/10.1073/pnas.1805062115. –E8124.

[38] T. Lee, S.H. Ko, S.J. Cho, R. Ryoo, Ultramicroporous carbon synthesis using lithium-ion effect in ZSM-5 zeolite template, Chem. Mater. 30 (2018) 6513–6520, https://doi.org/10.1021/acs.chemmater.8b03132.

[39] T. Kyotani, Z. Ma, A. Tomita, Template synthesis of novel porous carbons using various types of zeolites, Carbon 41 (2003) 1451–1459, https://doi.org/10.1016/S0008-6223(03)00090-3.

[40] D. Rojo-Gama, M. Nielsen, D.S. Wragg, M. Dyballa, J. Holzinger, H. Falsig, L. F. Lundegaard, P. Beato, R.Y. Brogaard, K.P. Lillerud, U. Olsbye, S. Svelle, A straightforward descriptor for the deactivation of zeolite catalyst H-ZSM-5, ACS Catal. 7 (2017) 8235–8246, https://doi.org/10.1021/acscatal.7b02193.

[41] I. Vollmer, S. Ould-Chikh, A. Aguilar-Tapia, G. Li, E. Pidko, J.L. Hazemann, F. Kapteijn, J. Gascon, Activity descriptors derived from comparison of Mo and Fe as active metal for methane conversion to aromatics, J. Am. Chem. Soc. 141 (2019) 18814–18824, https://doi.org/10.1021/jacs.9b09710.

[42] H. Park, J. Bang, S.W. Han, R.K. Bera, K. Kim, R. Ryoo, Synthesis of zeolite-templated carbons using oxygen-containing organic solvents, Microporous Mesoporous Mater. 318 (2021), 111038, https://doi.org/10.1016/j.micromeso.2021.111038.

[43] Y. Li, X. Wang, T. Thersleff, G. Svensson, N. Hedin, Silicoaluminophosphate (SAPO)-Templated activated carbons, ACS Omega 4 (2019) 9889–9895, https://doi.org/10.1021/acsomega.9b00135.

[44] I. Vollmer, M.J.F. Jenks, R. Mayorga González, F. Meirer, B.M. Weckhuysen, Plastic waste conversion over a refinery waste catalyst, Angew. Chem. Int. Ed. 60 (2021) 16101–16108, https://doi.org/10.1002/anie.202104110.

[45] M. Yoldi, E.G. Fuentes-Ordoñez, S.A. Korili, A. Gil, Zeolite synthesis from industrial wastes, Microporous Mesoporous Mater. 287 (2019) 183–191, https://doi.org/10.1016/j.micromeso.2019.06.009.
[46] H. Park, S.K. Terhorst, R.K. Bera, R. Ryoo, Template dissolution with NaOH–HCl in synthesis of zeolite-templated carbons: effects on oxygen functionalization and electrical energy storage characteristics, Carbon 155 (2019) 570–579, https://doi.org/10.1016/j.carbon.2019.09.020.
[47] C.S. Cundy, P.A. Cox, The hydrothermal synthesis of zeolites: history and development from the earliest days to the present time, Chem. Rev. 103 (2003) 663–701, https://doi.org/10.1021/cr020060i.